Simultaneous Multi-Object Segmentation using Local Robust Statistics and Contour Interaction

Yi Gao[1], Allen Tannenbaum[1,2], Ron Kikinis[3]

[1]Schools of Electrical Computer Engineering and Biomedical Engineering, Georgia Institute of Technology, Atlanta, GA, 30332.
[2]Department of EE, Technion-IIT, Haifa 32000, Israel.
[3]Surgical Planning Laboratory, Brigham & Women's Hospital, Harvard Medical School, Boston, MA 02115

Abstract. In this work, we present an active contour scheme to simultaneously extract multiple targets from MR and CT medical imagery. A number of previous active contour methods are capable of only extracting one object at a time. Therefore, when multiple objects are required, the segmentation process must be performed sequentially. Not only may this be tedious work, but moreover the relationship between the given objects is not addressed in a uniform framework, making the method prone to leakage and overlap among the individual segmentation results. On the other hand, many of the algorithms providing the capability to perform simultaneous multiple object segmentation, tacitly or explicitly assume that the union of the multiple regions equals the whole image domain. However, this is often invalid for many medical imaging tasks. In the present work, we give a straightforward methodology to alleviate these drawbacks as follows. First, local robust statistics are used to describe the object features, which are learned adaptively from user provided seeds. Second, several active contours evolve simultaneously with their interactions being governed by simple principles derived from mechanics. This not only guarantees mutual exclusiveness among the contours, but also no longer relies upon the assumption that the multiple objects fill the whole image domain. In doing so, the contours interact and converge to equilibrium at the desired positions of the given objects. The method naturally handles the issues of leakage and overlapping. Both qualitative and quantitative results are shown to highlight the algorithm's capability of extracting several targets as well as robustly preventing the leakage.

1 Introduction

Extracting anatomically and/or functionally significant regions from medical imagery, i.e., segmentation, is a challenge and important task in medical image analysis. One common practice consists of user initialization with one or several clicks (often called "seeds") in the target, and the algorithm then takes over to extract the desired object. A simple but intuitive example using such strategy is the region growing method [1]. Although the formalism is simple and straightforward, it reflects the two key roles of the user initialization: *Position*:

the positions of the initial seeds indicate the estimated position of the target; *Feature*: the image information in a given neighborhood of the seeds should be employed to learn the necessary characteristics of the desired object as well as to drive the segmentation. Nevertheless, original region growing only depends on the image intensity, and thus is many times not suitable for noisy and textured imagery. Furthermore, the segmentation boundary is not guaranteed to be as smooth as many times required. To address the first problem, Pichon *et al.* used robust statistics for better modeling of the image features at the locations of the seeds, and a fast marching algorithm to grow the segmentation contour [2]. Various active contour methods evolve a contour (curve or surface) in a variational manner to utilize both image information and contour geometry; see [3–11] and the references therein. The method proposed here follows this general philosophy, but in contrast to many active contour methods which only utilize the position information of the seeds, here we makes full use of the image information around the seeds in an adaptive fashion. Basically, the target object characteristics are learned online from the user inputs. Then the active contour evolves from the given places and converges to the desired boundary of the target.

Moreover, another desired feature for segmentation is the ability to simultaneously extract multiple objects. This can be quite advantageous in medical image analysis, where several related targets all need to be captured. However, most active contour algorithms are tailored to handle only one target at a time. Thus, the given algorithm needs to be executed sequentially several times in order to obtain the required multiple objects. However, since the individual segmentation processes do not interact with each other, it is difficult to guarantee mutual exclusiveness among contours. To address that, multiple object segmentation has been discussed in several papers [12–17]. In these works, the algorithms require the contours to be mutually exclusive (not overlapping). In addition, they also assume that the union of the regions bounded by the contours must be equal to the entire image domain. However, this is usually not a valid assumption for many medical imaging tasks. Our methodology does not rely on this assumption, which makes it more suitable for many medical imaging problems. This is accomplished by incorporating simple principles from mechanics into the contour interactions, which also handles the aforementioned problem of overlapping. Thus the algorithm naturally treats the issue of leakage. Moreover, researchers in [18, 19] used the shape prior to achieve the multiple target objective. However, not only that requires the learning data set and process for the shape prior, but also the mutual exclusiveness among the contours are not guaranteed.

2 Method

If we consider the segmentation process in our own visual system, we observe that when human is recognizing the objects in a scene, several basic steps take place in sequence [20]. We will illustrate this via an example. Suppose that we want to trace out the boundary of both the liver and the right kidney in medical imagery. First, prior anatomy knowledge drives our attention to the right abdominal region. Second, we focus at an area where we believe to be

most "liver-like," and learn the liver characteristics in this particular image. With such knowledge, we then move our focus to enclose more tissue that looks similar to those representative regions. Usually, such similarity ends when we reach a remote area. In particular, at the boundary where the liver touches the right kidney, the decision is difficult. Under such a situation, we apply a similar procedure to the kidney, and we come back to the same ambiguous region. However, this time with the information from both sides (liver and kidney), internally we perform a competition: we compare the current voxel with both the liver and the kidney to decide which boundary should advance, so the other should retreat. Finally, the boundaries of liver and kidney are placed at the balanced locations of the competition.

The segmentation scheme presented in this paper is a mathematical model for the above process. It is a semi-automatic method because the first step above is achieved by the user providing a label map indicating different targets by different labels. Each subsequent step is handled by an automatic algorithm and is detailed in what follows below.

2.1 Online feature learning

Denote the image to be segmented as $I : \Omega \to \mathbb{R}$ where $\Omega \subset \mathbb{R}^d$ is an open set and $d \in \{2, 3\}$. Likewise, the user provided label map is denoted as $L : \Omega \to \mathbb{N} \cup \{0\}$ where 0 indicates background and non-zero positive integers indicate the target object labels. For ease of discussion, in this paper, we assume the distinct labels to be consecutively ranging from 0 to N, an arbitrary positive integer. Moreover, the labeled region can be defined by several "clicks", and does not have to be close to the desired boundary. Next, voxels with the non-zero labels are categorized into different "seed groups" as $G_i = \{\boldsymbol{x} \in \Omega : L(\boldsymbol{x}) = i\}$.

In order to fully utilize the information given by the label map, we note that the seed group not only indicates the location of the target, but also provides some sample voxels contained in it. Hence, instead of making general assumptions on the target characteristics such as brighter/darker than surrounding area, we can learn them in an online fashion. Often times, the image intensity alone is not descriptive enough. Hence, a feature vector is extracted at each voxel, forming a feature image $\boldsymbol{f} : \Omega \to \mathbb{R}^{D_f}$. Subsequently, the segmentation is performed in the feature space. There are many choices for the feature vector such as wavelet coefficients, Fourier descriptors, Hessian matrix, etc. In this paper, we choose local robust statistics [21, 2] because they are not sensitive to image noise, and may be computed quickly.

To this end, for each voxel $\boldsymbol{x}$ in the image, we define the feature vector $\boldsymbol{f}(\boldsymbol{x}) \in \mathbb{R}^{D_f}$ by combining several robust statistics derived in a neighborhood $B(\boldsymbol{x}) \subset \Omega$ around $\boldsymbol{x}$. More explicitly, we denote $MED(\boldsymbol{x})$ as the intensity median within $B(\boldsymbol{x})$. In addition, the local intensity range is also an important characteristic, but is sensitive the noise. To address this issue, the distance between the first and third quartiles, namely the inter-quartile range ($IQR(\boldsymbol{x})$), is calculated as the second feature. Furthermore, the local intensity variance is a good candidate but again it is sensitive to outliers. In contrast, the median absolute deviation (MAD) is much more robust and is computed as $MAD(\boldsymbol{x}) := median_{\boldsymbol{y} \in B(\boldsymbol{x})}(I(\boldsymbol{y}) -$

$MED(\boldsymbol{x})$). Consequently, we define the feature vector $\boldsymbol{f}(\boldsymbol{x})$ as:

$$\boldsymbol{f}(\boldsymbol{x}) = (MED(\boldsymbol{x}), IQR(\boldsymbol{x}), MAD(\boldsymbol{x}))^T \in \mathbb{R}^3 \tag{1}$$

With the space of feature vectors thus defined, seed groups are now characterized by the probability density function of the feature vectors estimated by:

$$p_i(\boldsymbol{f}) = \frac{1}{|G_i|} \sum_{\boldsymbol{x} \in G_i} K_\eta(\boldsymbol{f} - \boldsymbol{f}(\boldsymbol{x})) \tag{2}$$

where K is the kernel function. In this work, we use the Gaussian kernel. Its variance is chosen to be η times the MAD of the seed group. η is preset to be 0.1, and we have found that this works for all the cases tested.

2.2 Contour evolution

To simplify the notation, we present the contour evolution in 2D. However it is noted that the method can be easily extended to 3D. In fact, all the experiments in Section 3 are in 3D. First, we denote the family of evolving closed contours as $C_i : [0, 1] \times \mathbb{R}^+ \to \mathbb{R}^2$. Without interactions among contours (interaction is addressed in Section 2.3 below), each contour evolves independently in order to minimize the energy functional:

$$E_i(C_i) := \int\limits_{\boldsymbol{x}\ in\ C_i} (p^c - p_i(\boldsymbol{f}(\boldsymbol{x})))d\boldsymbol{x} + \lambda \int_{C_i} ds \tag{3}$$

where p^c is the cut-off probability density used to prevent the contour leakage [22]. Likewise, $\lambda > 0$ is the smoothness factor. Computing the first variation of E_i and we obtain the flow of C_i:

$$\frac{\partial C_i(q,t)}{\partial t} = [p^c - p_i(\boldsymbol{f}(C_i(q,t))) + \lambda\kappa_i(q,t)]\, \boldsymbol{N}_i(q,t) \tag{4}$$

in which $\boldsymbol{N}_i$ is the inward unit normal vector field on C_i and κ_i is the curvature of the contour.

2.3 Contour interaction

Although the p^c term in equation (3) helps to prevent contour leakage, in many cases the result is not sufficiently satisfying. Indeed, it often results in the problem that certain regions are over-segmented, while some others are under-segmented. The leakage issue, i.e., making decisions in a transitional region, is sometimes a difficult task even for the human visual system. However, one particular strategy the visual system takes, is to approach the decision boundary from both sides by competition, rather than preventing the leakage from a single direction. To this end, we enable the interaction amongst the previously individually evolving contours using standard principles from Newtonian mechanics.

First, we regard the right hand side of equation (4) as the force applied on the infinitesimal curve segment at the position $C_i(q,t) =: \boldsymbol{p} \in \mathbb{R}^2$. Now with the interaction among curves, such a curve segment will also experience forces from other curves:

$$F_i^{ext}(\boldsymbol{p}) = -\sum_{j \neq i} \int_{C_j} e^{-|\boldsymbol{p}-C_j(w,t)|}(p_j(\boldsymbol{f}(\boldsymbol{p})) - p^c)\boldsymbol{N}_j(\boldsymbol{p})dw \tag{5}$$

Accordingly, the curve flow equation for C_i is now updated as:

$$\frac{\partial C_i(q,t)}{\partial t} = \left[p_i(\boldsymbol{f}(C_i(q,t))) - p^c - \lambda\kappa_i(q,t)\right]\boldsymbol{N}_i(q,t) + F_i^{ext}(C_i(q,t)) \tag{6}$$

The exponential term controls the "influence range" of the force. When curves are far away, this term reduces the F_i^{ext} effectively to zero. Moreover, using the "sparse field level set" implementation [23], the computation of F_i^{ext} is very efficient. In general, the contour evolution scenario is as follows: At the outset, the contours do not touch each other because the seeds are sparsely scattered in the domain. Thus each F_i^{ext} is approximately 0 and each contour evolves individually. As the evolution proceeds, the contours get closer and the mutual interactions begin to take place. Moreover, they will compete and finally rest at balanced (equilibrium) positions. Throughout the whole process, the contours are governed by the action/reaction principle from mechanics, and will never overlap with each other, which is a necessary feature for multi-object segmentation.

3 Implementation, Experiments and Results

Numerically, the contour evolution is implemented using the sparse field level set method for fast computation and flexibility in contour topology [23]. Moreover, in computing the robust statistics, the neighborhood size $B(\boldsymbol{x})$ is fixed at $3 \times 3 \times 3$. This value was used throughout all of our tests. Similarly, the p^c, λ in equations (6) are respectively fixed at 0.1, 0.3 for all of the tests. In what follows, we demonstrate the application of the proposed method in T1 weighted MR brain imagery and CT abdominal data, to illustrate the algorithm's robustness to the imaging modalities and noise. The results are also quantitatively evaluated.

3.1 Vervet brain segmentation

We first test on a T1 weighted MR images of the brain of vervets. In order to highlight the leakage problem as well as how the proposed multi-object scheme solves this problem, initially, only the white matter is segmented. As shown in Figure 1(a), the contour leakage gives a final result that contains not only white matter but also part of cerebellum. However, using the proposed method to segment several related objects gives the result shown in Figure 1(b). It can be seen that the final labeling of the cerebellum, shown in white, not only fully captures the cerebellum region, but also effectively prevents leakage from intruding into the white matter. Furthermore, we show the 3D views of the multiple segmented

objects: white matter, cerebellum, and ventricle. To highlight the region where the contour interaction between the white matter and cerebellum helps prevent leakage, we show the view from both posterior and inferior. It can be observed that there is no intersection between the contours. In particular, the cerebellum contour nicely "pushes" the white matter contour out, and so prevents leakage into the cerebellum.

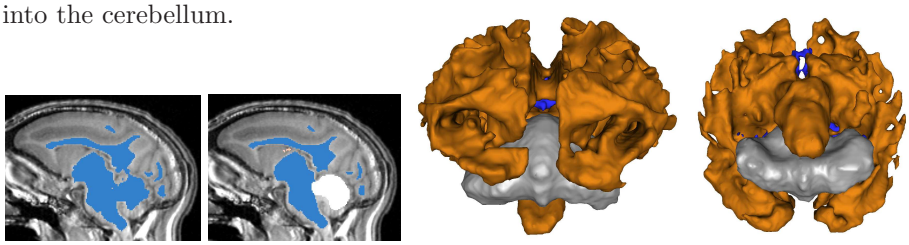

(a) (b) (c) (d)

Fig. 1. In Subplot 1(a), we only segment one object (white matter). However, the contour leaks into part of cerebellum and part of brain stem. In 1(b), when segmenting several objects simultaneously, the white label for cerebellum effectively prevents the leakage. 3D plots include posterior 1(c) and inferior 1(d) views. It can be observed that there is no intersection between the surfaces.

3.2 Quantitative analysis for ventricle and caudate nucleus

In this second experiment, we extract both the ventricle and the caudate nucleus from MR images and present the results both qualitatively and quantitatively. In the experiment, the caudate nucleus is a difficult object to extract due to the poor contrast with its surrounding tissues. In fact, if we only place seeds in the caudate, we get the result shown in Figure 2(a) where the large leakage is circled. On the other hand, if we also places some seeds around caudate, we also capture some portion of white matter as shown in Figure 2(b) in almond color. Simultaneously, the caudate shape is kept intact and no leakage occurs. The almond part can be discarded because the caudate is the only object of interested and the final result is shown in Figure 2(c).

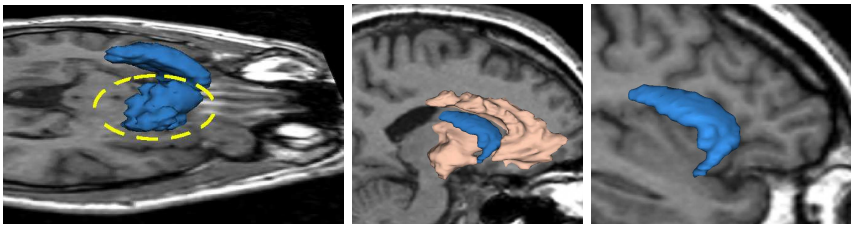

(a) (b) (c)

Fig. 2. If only place seeds in caudate we get segmentation in Subplot 2(a) where the leakage is circled in yellow (viewing from superior-right). After putting some auxiliary seeds in the surrounding tissue we get results in the sagittal view in 2(b) where the caudate shape is kept intact. Discarding the auxiliary region and the caudate is shown alone in 2(c). (Sagittal view from right.)

Performing the same scheme on another subject gives the results in Figure 3(a) and 3(b) where we show both the segmentation and the original image. In addition to the caudate, the method is also applied on ventricle which is

an easier segmentation task. In total, we performed 10 tests on different subjects. The Dice coefficients are computed against expert segmentations, and are plotted in Figure 3(c).

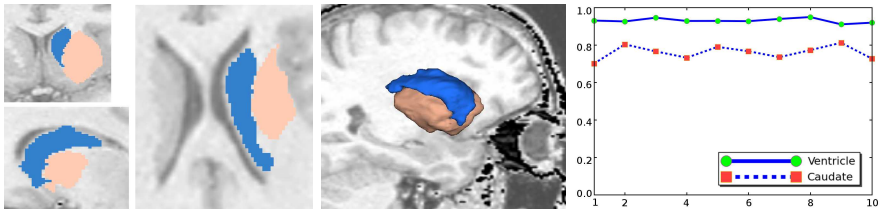

(a) (b) (c)

Fig. 3. Subplot 3(a) and 3(b) overlay the segmentation results on the original images. The almond region is again auxiliary for preventing leakage. Subplot 3(c) shows the Dice coefficients of segmenting 10 ventricles and caudates, comparing with expert segmentation.

3.3 Abdominal organ segmentation

The proposed algorithm is general purposed and can be used for many different tasks. Indeed, although the previous examples only utilize the multi-object segmentation capability for leakage prevention, in the last experiment, 11 different organs/tissues are extracted from an abdominal CT image. The size of the image is $512 \times 512 \times 204$ and the running time on a machine with 3.0GHz Intel Core 2 Quad CPU and 8G memory is about 8 minutes. The result is shown in Figure 4.

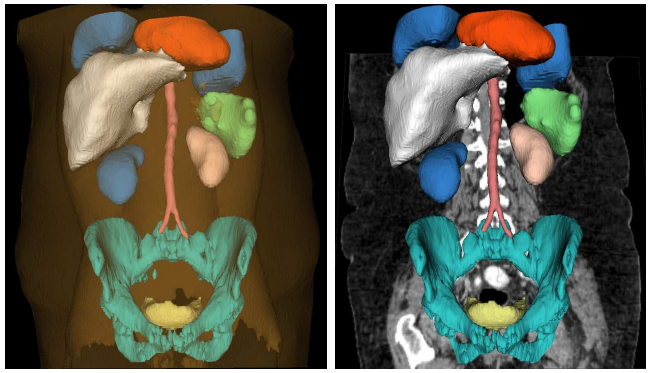

(a) (b)

Fig. 4. Segmentation of heart, two lungs, liver, two kidneys, spleen, abdominal aorta, pelvis, bladder, skin/muscle/fat. The subplot 4(b) removes skin/muscle/fat but overlays the original image.

4 Conclusions and Future Work

In this note, we proposed a general-purpose image segmentation scheme for medical data. In particular, the image features are extracted using certain local robust statistics as the segmentation criterion. Subsequently, the object characteristics are learned from the user initialization which is further used to guide the active contour evolution in a variational framework. Furthermore, we incorporate the

interactions between the contours into the evolution motivated by simple principles from mechanics. This not only effectively reduces the contour leakage, but also results in a multi-object segmentation scheme without assuming that the union of the segmentation regions is the entire the whole domain.

Future work includes exploring more choices for the image features, such as Fourier/wavelet descriptors. Furthermore, we will incorporate shape priors for the multiple targets. Combined with the contour interaction, this is expected to further improve our results.

References

1. Sonka, M., Hlavac, V., Boyle, R.: Image Processing, Analysis, and Machine Vision Second Edition. International Thomson (1999)
2. Pichon, E., Tannenbaum, A., Kikinis, R.: A statistically based flow for image segmentation. Medical image analysis **8**(3) (2004) 267–274
3. Kass, M., Witkin, A., Terzopoulos, D.: Snakes: Active contour models. IJCV **1**(4) (1988) 321–331
4. Malladi, R., Sethian, J., Vemuri, B., et al.: Shape modeling with front propagation: A level set approach. IEEE TPAMI **17**(2) (1995) 158–175
5. Kichenassamy, S., Kumar, A., Olver, P., Tannenbaum, A., Yezzi, A.: Gradient flows and geometric active contour models. In: IEEE ICCV. (1995) 810
6. Caselles, V., Kimmel, R., Sapiro, G.: Geodesic active contours. IJCV **22**(1) 61–79
7. Yezzi, A., Kichenassamy, S., Kumar, A., Olver, P., Tannenbaum, A.: A geometric snake model for segmentation of medical imagery. IEEE TMI **16**(2) (1997) 199–209
8. Yezzi Jr, A., Tsai, A., Willsky, A.: A statistical approach to snakes for bimodal and trimodal imagery. In: IEEE ICCV. Volume 2. (1999)
9. Chan, T., Vese, L.: Active contours without edges. IEEE TIP **10**(2) (2001) 266–277
10. Michailovich, O., Rathi, Y., Tannenbaum, A.: Image segmentation using active contours driven by the bhattacharyya gradient flow. IEEE TIP **16**(11) 2787
11. Lankton, S., Tannenbaum, A.: Localizing Region-Based Active Contours. IEEE TIP **17**(11) (2008) 2029–2039
12. Zhu, S., Yuille, A.: Region competition: Unifying snakes, region growing, and bayes/MDL for multiband image segmentation. IEEE TPAMI **18**(9) (1996) 884
13. Brox, T., Weickert, J.: Level set segmentation with multiple regions. IEEE TIP **15**(10) (2006) 3213
14. Vese, L., Chan, T.: A multiphase level set framework for image segmentation using the Mumford and Shah model. IJCV **50**(3) (2002) 271–293
15. Grady, L.: Random walks for image segmentation. IEEE TPAMI **28**(11) 1768
16. Zhao, H., Chan, T., Merriman, B., Osher, S.: A Variational Level Set Approach To Multiphase Motion. Journal of computational physics **127**(1) (1996) 179–195
17. Shi, J., Malik, J.: Normalized cuts and image segmentation. IEEE TPAMI **22**(8) (2000) 888–905
18. Yan, P., Shen, W., Kassim, A., Shah, M.: Segmentation of neighboring organs in medical image with model competition. MICCAI 2005 270
19. Yang, J., Staib, L., Duncan, J.: Neighbor-constrained segmentation with level set based 3-D deformable models. IEEE TMI **23**(8) (2004) 940
20. Palmer, S.: Vision science: Photons to phenomenology. MIT press (1999)
21. Huber, P., Ronchetti, E.: Robust statistics. Wiley-Blackwell (2009)

22. Yang, Y., Tannenbaum, A., Giddens, D., Coulter, W.: Knowledge-based 3D segmentation and reconstruction of coronary arteries using CT images. In: IEEE EMBS. (2004) 1664–1666
23. Whitaker, R.: A level-set approach to 3D reconstruction from range data. IJCV **29**(3) (1998) 231